mTORC2-mediated cell-cell interaction promote BMP4-induced WNT activation and mesoderm differentiation

Li Tong,[1,3] Faiza Batool,[1,3] Yueh-Ho Chiu,[1,3] Yudong Zhou,[1] Xiaolun Ma,[1] Santosh Atanur,[2] Wei Cui[1*]

[1]Institute of Reproductive and Developmental Biology, Department of Metabolism, Digestion and Reproduction, Faculty of Medicine, Imperial College London, W12 0NN, UK;

[2]Section of Genetics and Genomics; Department of Metabolism, Digestion and Reproduction, Faculty of Medicine, Imperial College London, W12 0NN, UK

[3]These authors contributed equally: Li Tong, Faiza Batool, Yueh-Ho Chiu.

[*]Correspondence: Institute of Reproductive and Developmental Biology, Faculty of Medicine, Imperial College London, Du Cane Road, London W12 0NN, UK. wei.cui@imperial.ac.uk.

Abstract

The mechanistic target of rapamycin complex 2 (mTORC2) is essential for embryonic development but the underlying molecular mechanisms remain unclear. Here we show that disruption of mTORC2 in human embryonic stem cells (hESCs) considerably alters the balance of Rho/Rac signaling and reduces cell adhesion. Although these changes have no clear effect on hESC self-renewal and the expression of pluripotent markers, they significantly avert BMP-induced activation of canonical WNT genes, leading to impaired mesendoderm differentiation. Direct activation of downstream WNT pathway by inhibiting GSK3 dramatically improves mesendoderm differentiation in mTORC2-deficient hESCs. Our study uncovers a new mechanism by which mTORC2 regulates cell fate determination and, more importantly, link the intercellular contacts with the activation of the WNT genes.

Key Words

mTORC2, WNT, BMP4, human embryonic stem cells, mesoderm/endoderm differentiation, cell adhesion, cell-cell interaction,

Introduction

The mechanistic/mammalian target of rapamycin (mTOR) is a serine/threonine protein kinase that is evolutionarily conserved in all eukaryotes and acts through two distinct multiprotein complexes, mTORC1 and mTORC2, in the homodimerized form[1-3]. Although both mTORC1 and mTORC2 contain mTOR as the catalytic subunit and mammalian lethal with SEC13 protein 8 (mLST8), each complex also contains its specific components. RAPTOR (regulatory-associated protein of mTOR) is specific to mTORC1 and is replaced by RICTOR (rapamycin-insensitive companion of mTOR) and mSIN1 (mammalian stress-activated map kinase-interacting protein 1) in mTORC2. These complex-specific components dictate distinct regulatory mechanisms, substrates, and functions of the complexes[4]. The mTOR signaling overall plays an important role in cell proliferation, cytoskeleton remodeling and cell metabolism; hence, it is essential for embryonic development and tissue homeostasis[5]. In the last decades, studies in mTORC1 have significantly advanced our knowledge of mTORC1[4,6], while functions and underlying molecular mechanisms of mTORC2 remain ambiguous due to complicated crosstalk and interwoven regulatory machineries with other pathways as well as a lack of mTORC2-specific inhibitors.

Loss-of-function studies in mice demonstrate that mTORC2 is vital for embryonic development as disrupting either Rictor or mSin1 leads to embryonic lethality at E10-11 due to vasculature defects[7,8]. This is later than the death of Raptor-null embryos at E6.5, suggesting that mTORC1 and mTORC2 have diverse functions in embryonic development. Intriguingly, the phenotypes of tissue-specific mTORC2 knockout in mice, including endothelial cells, are very mild, showing no developmental defects, unless the disruption occurs around gastrulation, causing embryonic lethality at mid-gestation, similar to that of germline knockout[9-16]. These data imply that mTORC2 may have an important function during early embryonic development, particularly around gastrulation. However, the underlying molecular mechanisms are largely unknown. In addition to embryonic development, the role of mTOR signaling, especially mTORC2, in the maintenance and differentiation of pluripotent stem cells (PSCs) also remains elusive[17,18].

Seeking to explore the underlying mechanisms by which mTORC2 regulates embryonic development and cell fate determination, we disrupted the expression of *RICTOR* in human embryonic stem cells (hESCs) by CRISPR/Cas9. Although mTORC2-deficiency does not affect self-renewal and the expression of pluripotent markers, *RICTOR* knockout (RIC-KO) hESCs exhibit a considerable reduction in cell adhesion and cell-cell interaction, showing dramatic impairment in mesoderm and endoderm differentiation. Using the BMP4-induced

mesoderm differentiation model, we further demonstrate that mTORC2-regulated intercellular adhesion is important for the activation of WNT genes and subsequent WNT signaling, a key pathway for mesendoderm differentiation.

Results

Eradicating mTORC2 signaling in hESCs shows no effect on the overall expression of pluripotent markers

The gene *RICTOR* was disrupted in H1 hESCs using CRISPR/Cas9 and several RIC-KO clones were obtained after two rounds of sequential clonal isolation with two clones, K1 and K5, being expanded (Supplementary Fig. 1a,b). As reported previously, elimination of RICTOR dramatically reduced mSIN1 protein in these cells[19], while the expressions of other core components of mTOR complexes were not affected (Fig. 1a). Correspondingly, mTORC2 activity was diminished, but the activities of mTORC1 and PI3K-PDK1 were maintained (Fig. 1b). During clonal isolation and initial expansion, RIC-KO hESCs had a transient reduction in cell growth compared to wildtype (WT) controls but this proliferative reduction gradually diminished. By the time clonal lines were established, RIC-KO hESCs revealed faster growth than WT controls with less cell death possibly due to an increased level of MAPK-ERK pathway (Fig. 1c; Supplementary Fig. 1c). However, the growth in RIC-KO hESCs became slower than WT controls after their differentiation into fibroblasts (Fig. 1c), which is consistent with the data obtained from mouse embryonic fibroblasts (MEF) derived from *Rictor*-null mice[7,8]. Both RIC-KO hESC lines contained the correct number of chromosomes and showed similar results in alkaline phosphatase-positive colony formation, although their colonies appeared less compact compared to WT hESCs (Supplementary Fig. 1d,e; Fig. 1d). The core pluripotent transcription factors, OCT4, SOX2 and NANOG, and hESC-associated cell surface antigens, SSEA4 and Tra-1-81, retained their expression in RIC-KO hESCs (Fig. 1e-h).

To circumvent off-target effects of sgRNAs and avoid cell line-dependent bias, the expression of *RICTOR* was also disrupted in H7 hESCs through shRNA-medicated knockdown (RIC-KD) (Supplementary Fig. 1f,g). Resulting H7 RIC-KD hESCs further confirmed this dynamic pattern of proliferation/growth, which they initially grew slower but later surpassed their WT controls, after mTORC2 disruption (Supplementary Fig. 1h). H7 RIC-KD hESCs revealed similar colony morphology and pluripotent marker expression as H1 RIC-KO hESCs (Supplementary Fig. 1i,j). Together, these data demonstrate that disruption of *RICTOR* in hESCs only abolishes mTORC2 activity without clear effect on

mTORC1 and PI3K-PDK signaling and that mTORC2 signaling is not necessarily required for the maintenance of self-renewal and the expression of pluripotent markers in hESCs.

mTORC2 deficiency in hESCs significantly reduces cell adhesion and alters RhoA/Rac signaling

In our routine cultures, hESCs were propagated by collagenase-assisted mechanical dissection and the resulting small clumps of cells were directly plated onto Matrigel-coated culture plates[20]. Although disruption of *RICTOR* in hESCs showed no apparent effect on self-renewal and the expression of pluripotent markers, it was noticeable that these cells exhibited a much lower ability of cell attachment than WT controls (Fig. 2a, upper). Application of 10 μM ROCK inhibitor Y-27632 (ROCKi hereafter) visibly improved the attachment of RIC-KO hESCs (Fig. 2a, lower). This was supported by quantitative analysis of single-cell plating assays in both H1 RIC-KO and H7 RIC-KD (together called RICTOR-deficient, RIC-DF) hESCs (Fig. 2b; Supplementary Fig. 2a). Furthermore, proteins associated with intercellular complexes, such as E-cadherin (E-CAD) and ZO1, also revealed reduced expression in RIC-DF hESCs despite their transcripts not showing a significant decrease (Fig. 2c,d; Supplementary Fig. 2b-d). Although β-CATENIN (β-CAT) protein expression did not exhibit a clear reduction in RIC-KO hESCs, its localization in RIC-KO hESCs was less at the plasma membrane. These data concurred with the observation that RIC-DF hESC colonies were less compact than those of WT controls (Fig. 1d and Fig. S1i), suggesting reduced cellular interactions in RIC-DF hESCs.

The impeded cellular interactions in RIC-DF hESCs became more evident when these cells were subjected to the embryoid body (EB) formation assay which was performed by seeding single hESCs into the AggreWell plates in the presence of ROCKi initially. In WT hESCs, ROCKi was only necessary on the first day to assist the formation of aggregates, and then the aggregates could grow in suspension to form EBs in the absence of ROCKi (Supplementary Fig. 2e). By contrast, RIC-DF hESCs required ROCKi throughout the EB formation; otherwise, the aggregates gradually disintegrated after the withdrawal of ROCKi (Fig. 2e). Trypan blue staining of these dissociated cells was negative, indicating their viable nature. Even in the presence of ROCKi, RIC-DF EBs showed more blebbing on the surface of EBs (Fig. 2e; Supplementary Fig. 2f). These results demonstrate that RICTOR/mTORC2-deficiency significantly hinders both cell-ECM (extracellular matrix) and cell-cell interactions.

Since the application of ROCKi in RIC-DF hESCs could recover, at least partly, cell-ECM and cell-cell interactions, upregulation of RhoA-ROCK signaling was thought to account for altering cell adhesion in these cells. Indeed, RhoA activity showed a significant increase in RIC-DF hESCs compared to that of their WT controls (Fig. 2f; Supplementary Fig. 2g).

Conversely, Rac1-GTP, the active form of Rac1, was expressed at lower levels in RIC-DF hESCs (Fig. 2g; Supplementary Fig. 2h). Moreover, the phalloidin staining also revealed an altered pattern of F-ACTIN in RIC-KO hESCs, implying a change in cytoskeleton (Supplementary Fig. 2b). It is well-known that RhoA and Rac1 antagonize each other, and they coordinately maintain the homeostasis of cell adhesion, cytoskeleton, and movement[21,22]. Our data suggest that mTORC2 plays an important role in the regulation of RhoA-ROCK/Rac1 signaling pathways in hESCs and that disruption of mTORC2 considerably upregulates RhoA-ROCK, impeding cell adhesion.

Transcriptomic analysis reveals downregulation of genes associated with mesoderm differentiation and WNT signaling in RIC-KO hESCs

RNA-seq analysis of WT (C1 & C3) and RIC-KO (K1 &K5) hESCs showed that majority of genes exhibited similar expression patterns and that only 0.6% of genes (195 out of 32673) were differentially expressed between the two groups (2-fold up or down, $p_{adj} < 0.05$) with 140 of them downregulated and 55 genes upregulated (Fig. 3a,b; Supplementary Fig. 3a; Supplementary Table 1,2). It was noted that the downregulated genes included several transcription factors that regulate lineage specification, particularly mesoderm and endoderm, such as *GATA4*, *FOXA2, SOX17 and SP5*[23-25], while the transcription factors that are responsible for maintaining pluripotency or promoting neural differentiations were expressed similarly between WT and RIC-KO hESCs (Fig. 3b; Supplementary Fig. 3b). Gene ontology (GO) enrichment analysis revealed that the downregulated genes were predominantly involved in embryonic development, embryo patterning, and muscle development and were likely through the regulation of gene expression and growth factor/cytokine activity (Fig. 3c,d; Supplementary Table 3). Several genes were linked to the regulation of WNT signaling by KEGG pathway (Fig. 3e). The upregulated genes showed no statistically significant results. These data suggest that mTORC2 deficiency in hESCs might affect their cell fate specification.

Disruption of mTORC2 hinders mesoderm and endoderm differentiation

To assess pluripotency of RIC-DF hESCs, embryoid body (EB)-mediated differentiation was performed in the presence of ROCKi (Supplementary Fig. 2e) and showed that both WT and RIC-DF hESC-derivatives encompassed cells of all three germ layers (Fig. 4a; Supplementary Fig. 4a). However, it was clearly visible that the proportions of mesodermal and endodermal cells were less in RIC-KO EBs than in WT controls (Fig. 4a). This was supported by quantitative mRNA analysis, showing that mesoderm (*BRACHYURY*, *TBX6* and *FLK1*) and endoderm (*FOXA2*, *GATA6* and *SOX17*) transcripts were expressed at much lower levels in RIC-KO EBs, whereas neural progenitor genes (*PAX6*, *SOX1* and *BRN2*)

revealed higher expression in these cells (Fig. 4b). Differentiation of H7 RIC-KD hESCs generated a similar outcome, albeit the difference being moderate due to partial silencing of the shRNA transgene during differentiation (Supplementary Fig. 4a,b).

Since both mesoderm and endoderm differentiation were affected, we assumed that mTORC2-deficiency might affect hESCs differentiation into mesendoderm, a common precursor of both lineages, resembling the bipotent population in a gastrulating embryo[26]. Thus, we focused our study on this population, adapting a BMP-induced mesoderm differentiation approach in 2D-colony and 3D-spheroid cultures and using BRACHYURY positive (BRA+) cells as a marker given its high expression in these cells (Fig. 4c,e)[27,28]. After 48-hour BMP4 induction, control WT hESCs exhibited symmetry breaking during differentiation in both 3D spheroids and 2D colonies as previously reported that BRA+ cells were predominantly at one side of a spheroid or colony while SOX2 positive cells at the opposing side (Fig. 4d, left and 4f, left)[28]. By contrast, significantly fewer BRA+ cells were detected in RIC-KO cultures than in corresponding WT controls (Fig. 4d, right and 4f, right). Furthermore, the expression of mesoderm/endoderm genes was also higher in WT than RIC-KO cells, confirming a reduction of mesendoderm differentiation in RIC-KO hESCs (Supplementary Fig. 4c). These results demonstrate that ablation of mTORC2 in hESCs considerably impeded their differentiation into mesendoderm, implying that mTORC2 signaling has a role in the regulation of mesendoderm differentiation.

Activation of WNT signaling resumes mesendoderm differentiation in RIC-KO hESCs

Next, we sought to explore the underlying mechanisms by which mTORC2 regulates mesendoderm differentiation. Since 3D spheroids and 2D colonies produced similar results in BMP4-induced differentiation, we carried out further experiments in 2D colonies. It has been well studied that BMP, Wnt and Nodal pathways are the key to orchestrate gastrulation in murine embryos wherein BMP4 from extraembryonic tissues stimulates epiblasts to activate Wnt signaling, which then enhances Nodal, and together they promote the formation of primitive streak and mesendoderm (Supplementary Fig. 5a)[29]. Anatomical and molecular analysis of monkey embryos suggest that the key regulatory mechanisms driving gastrulation are conserved between species[30]. Thus, we first activated all three pathways by treating hESCs with BMP4 together with GSK3 inhibitor CHIR99021 (CHIR) to activate WNT signaling and Activin A (AA) to simulate the activation of NODAL (Supplementary Fig. 5b). This combined treatment substantially increased BRA+ cells in RIC-KO colonies, leading to a higher proportion of BRA+ cells than that in WT controls per colony (Fig. 5a). The data suggest that the RIC-KO hESCs are competent to generate BRA+ cells and that mTORC2-deficiency possibly disrupt BMP4-induced activation of WNT or/and NODAL pathways,

resulting in defective mesendoderm differentiation. To test this hypothesis, we then treated RIC-KO and WT hESCs with BMP4 in combination with either CHIR or AA to dissect the signaling involved. Remarkably, addition of AA revealed a similar outcome as BMP4 alone, showing a significant reduction of BRA+ cells in RIC-KO cells (Fig. 5B), whereas the addition of CHIR dramatically increased BRA+ cells in both WT and RIC-KO hESCs and there were no significant differences between them (Fig. 5c). These results suggest that mTORC2-deficiency impedes mesendoderm differentiation by encumbering BMP4-induced activation of WNT signaling and that WNT signaling is essential for driving mesendoderm differentiation.

In supporting this, treating hESCs with CHIR alone also showed no difference in BRA+ cells between WT and RIC-KO hESCs (Fig. 5d). Interestingly, when comparing various treatments in the same cell lines, we noted that the addition of AA with BMP4 did not significantly increase the percentage of BRA+ cells (BMP4+AA vs BMP4) in both WT and RIC-KO hESCs, whereas AA clearly suppressed BRA+ cells induced by BMP4 and CHIR together (BMP4+AA+CHIR vs BMP4+CHIR) in WT hESCs, but not RIC-KO hESCs (Supplementary Fig. 5c). The reduction of BRA+ cells by the addition of AA with BMP4+CHIR in WT cells could be due to the ability of AA to promote BRA+ cells into the endoderm lineage after WNT priming process[31], while the absence of mTORC2 in RIC-KO cells might inhibit AA-induced endoderm differentiation. The upregulation of the MAPK-ERK pathway in RIC-KO cells might account for the inhibition of AA signaling and endoderm differentiation[32]. Together, these results corroborate that mTORC2 regulates BMP4-induced mesendoderm differentiation mainly through modulating the activation of WNT signaling.

mTORC2-deficiency suppresses BMP4-induced expression of WNT genes in hESCs

Since GSK3 inhibitor is able to restore BMP4-induced mesendoderm differentiation in RIC-KO hESCs (Fig. 5), we anticipated that mTORC2-deficiency may affect WNT pathway upstream of GSK3. Although mTORC2 is reported to maximize AKT activity that can exert inhibitory phosphorylation on GSK3 and subsequently enhances WNT signaling[33], phosphorylation of GSK3 was similar between WT and RIC-KO hESCs (Fig. 6a; Supplementary Fig. 6a), which was consistent with the findings in mTORC2-null mice[7]. The absence of phosphorylation of PKCζ-turning motif and PKCζ protein confirmed that mTORC2 remained inactive throughout the differentiation (Fig. 6a). We next investigated gene expression associated with the WNT signaling during BMP4-induced differentiation (Fig. 6b). The BMP4 treatment induced significantly higher expression of canonical WNT genes, *WNT3, WNT3A* and *WNT8A*, in WT than RIC-KO cells. Consistently, the WNT target genes, *AXIN2* and *LEF1*, also showed higher expression in WT cells (Fig. 6a,b). This

evidence demonstrated that BMP4-induced WNT activation was suppressed in RIC-KO hESCs, which likely accounted for the reduced WNT signaling and impeded mesendoderm differentiation in these cells.

It has been reported that the BMP4 receptors are expressed at the basolateral sides of cells, herein only the cells at the edge of a colony are accessible to BMP4 in the media due to intercellular junctions and that E-CAD may modulate WNT signaling patterning in hESCs[34-36]. Since the RIC-KO hESCs exhibited a clear reduction in E-CAD expression and cell-cell interactions (Fig. 2), we investigated whether these could affect BMP4 and WNT signaling during BMP4-induced differentiation. Although both WT and RIC-KO hESCs revealed a considerable increase in phosphorylation of SMAD1/5/9 (briefed as pSMAD1, hereafter), the activated form of BMP4 effectors, at 1-hour post-BMP4 stimulation, the phosphorylation was dramatically reduced from 24 hours onward in RIC-KO cells but maintained at a certain level in WT controls (Fig. 6a). Higher upregulation of the BMP4 antagonist NOGGIN in RIC-KO hESCs might suppress BMP4 signaling (Supplementary Fig. 6b), and moreover, the upregulation of MAPK-ERK in RIC-KO hESCs could also promote the degradation of active Smad1 signals[37]. Intriguingly, pSMAD1 also revealed distinct patterning in WT and RIC-KO hESCs and the pattern in WT cells associated with E-CAD expression (Fig. 6c; Supplemenary Fig. 6c). More importantly, LEF1 showed the similar dynamic pattern as pSMAD1 in WT hESCs, which was initially near the boundary of strong E-CAD+ area at 24 hours and then was spread to the E-CAD+ area, while it was detected only in a few cells in RIC-KO colonies (Fig. 6d, Supplementary Fig. 6d). Collectively, these findings suggest that cell-cell interactions may play an important role not only in the formation of the BMP4 signaling gradient but also in the activation of WNT genes.

Elimination of cell-cell interaction diminishes BMP4-induced upregulation of WNT genes in hESCs

To further validate if cellular interaction is crucial for BMP4-induced activation of WNT genes and mesendoderm differentiation in hESCs, we performed this differentiation in WT hESCs that were seeded either in colonies (CL) or in single cells (SC) (Fig. 7a). While asymmetrically distributed BRA+ cells were detected in CL cultures at 48 hours of BMP4 treatment as expected, hardly any BRA+ cells appeared in SC cultures (Fig. 7b). Furthermore, pSMAD1 signals were evenly distributed in SC cultures and no membrane-bound E-CAD were detected in these cells (Fig. 7c). The expression of canonical WNT and WNT target genes was lower in SC than in CL cultures and correspondingly, mesendoderm markers were expressed much lower in SC than in CL cultures (Fig. 7d; Supplementary Fig. 7a). These data support the notion that BMP4-induced mesendoderm differentiation requires

close cell-cell contact and that cellular interaction is vital for BMP4-induced activation of WNT genes in hESCs. Moreover, the combined BMP4 treatment with CHIR and AA in these SC cultures efficiently produced BRA+ cells (Supplementary Fig. 7b), proving that a lack of cell-cell interaction accounts for defective WNT activation and mesendoderm differentiation in response to BMP4.

Taken together, our results demonstrate that mTORC2 controls mesoderm and endoderm differentiation of hESCs through regulating intercellular connection, a crucial factor that mediates BMP4-induced expression of WNT genes and subsequently activation of WNT signaling.

Discussion

In this study, we investigated the role of mTORC2 in the regulation of PSC properties using *RICTOR*-deficient hESCs and show that mTORC2-deficient hESCs can retain their self-renewal and pluripotency in an undifferentiated state. The studies are carried out with two RIC-KO H1 clones and two RIC-KD H7 hESC lines, thus excluding clonal or cell line-specific bias. Although a transient reduction in proliferation is observed at the early stage of the mTORC2-deficient hESCs, they recover and grow even faster after extended culture without clear genetic changes, suggesting an adaptive growth ability in hESCs, possibly via upregulation of FGF-MAPK-ERK signaling. However, mTORC2-deficiency in hESCs reduces cellular interaction and impairs the mesendoderm differentiation. Although our findings agree with a recent report that *RICTOR*-knockout H9 hESCs hinders mesoderm differentiation, the RIC-KO H9 hESCs have a reduced ability of self-renewal[38]. This discrepancy is unlikely due to different genetic backgrounds as both H1 and H7 hESC lines in our studies revealed similar phenotypes after eliminating mTORC2. We believe that different culture conditions, MEF-conditioned medium (MEF-CM) used in our studies versus the chemically defined medium mTeSR in their studies, might account for the discrepancy as our RIC-KO hESCs also became gradually differentiated in mTeSR. While the mechanisms for this difference require further investigation, it is possible that MEF-CM, but not mTeSR, contains ECM and extracellular vesicles produced by MEF, which may compensate, at least partly, for the reduced intercellular communication in mTORC2-deficient hESCs, facilitating the maintenance of undifferentiation[39,40]. Therefore, our results demonstrate that mTORC2 is not necessarily required for the maintenance of hESCs.

The Rho family of GTPase has determinant roles in cell adhesion and epithelial morphogenesis[41,42] and our studies show that mTORC2-deficiency in hESCs results in

increased RhoA-GTP and decreased Rac1-GTP, leading to aberrant cell adhesion. Notably, the application of Rho-ROCK inhibitor significantly improves this condition. It has been reported that RhoA and Rac1 activities can be regulated by mTORC2 and its substrates, particularly PKC, through phosphorylation of RhoA/Rac regulators, including Rac1-specific guanine nucleotide exchange factor (GEF), RhoGDI2 and p190RhoGAP[43-45]. Disruption of mTORC2 causes PKC misfolding and degradation, abolishing its expression in hESCs[46], which could affect Rho/Rac1 signaling in these cells. Furthermore, RICTOR is reported to suppress RhoGDI2 independent of mTORC2 activity to maintain Rac1 GTPase activity[47]. Therefore, RICTOR/mTORC2 can affect Rho/Rac GTPase activities through multiple pathways.

A main finding of our study is that mTORC2-deficiency considerably impedes hESC differentiation into mesoderm and endoderm lineages. Furthermore, we demonstrate that mTORC2-deficiency does not affect the intrinsic competence of hESCs to generate BRA+ cells but significantly attenuates the activation of canonical WNT genes, subsequently suppressing WNT signaling in response to BMP4 stimulation. Forced activation of the WNT/β-CATENIN pathway in RIC-KO hESCs completely rescues mesendoderm differentiation, corroborating the essential role of WNT signaling in mesendoderm differentiation and gastrulation[48]. More importantly, we show that cellular interaction appears to be necessary for the BMP-induced upregulation of canonical WNT genes in hESCs. Although the regulation of WNT signaling has been intensively studied, the focus is predominantly on downstream effector β-CATENIN and only limited reports are on the regulatory mechanisms of upstream ligands of WNT genes. The p53 family has been shown to directly activate the *Wnt3* gene in mouse ESCs to promote their mesendoderm differentiation[49], and the YAP protein can bind to an intragenic enhancer of the *WNT3* gene in hESCs to prevent its premature activation by Activin-induced SMAD2/3[50]. Here we show that mTORC2-mediated cell-cell interactions are important for BMP-induced activation of canonical WNT genes and cell patterning during early differentiation and development. The exact mechanisms of what triggers WNT gene activation and whether the activation is related to p53 or YAP await further investigation.

In addition to the effect of mTORC2 on WNT activation, it is interesting to note that mTORC2 may also affect TGFβ signaling, independent of WNT, in the endoderm specification. This notion is supported by the transcriptomic profiles in WT and RIC-KO hESCs, in which a large proportion of downregulated genes in RIC-KO hESCs are associated with BMP/TGFβ-induced mesoderm/endoderm differentiation. Moreover, the expression of pSmad1 induced by BMP4 shows an accelerated decline in KO than WT cells and the addition of AA into BMP4+CHIR cultures only reduces the differentiation of BRA+ cells in WT but not KO

hESCs. However, these results differ from our previous report that inhibiting mTORC2 in RPMI medium promotes AA-induced endoderm differentiation[51]. Two different culture media likely account for the discrepancy between the experiments as different environments will considerably influence the outcome of mTORC2 on TGFβ signaling through distinct crosstalks[52]. Therefore, the effect of mTORC2 on TGFβ/BMP signaling is cell context-dependent[32]. Nonetheless, our finding that cell-cell interaction has a role in activation of WNT genes and WNT signaling may have an important implication beyond ESC differentiation.

Mesendoderm differentiation resembles, to a certain extent, the primitive streak formation during gastrulation. Although mTORC2-deficient hESCs exhibit defects in mesendoderm differentiation, mTORC2-null mouse embryos undergo successful gastrulation to generate the three germ layers[7,8]. It is possible that rapid proliferation of epiblast and limited space in post-implantation embryos may mechanically force the physical contacts between epiblast cells so that gastrulation can proceed. Additionally, maternal factors could also play a role during this early development. Therefore, the effects of RICTOR/mTORC2 in differentiation and development are complex, which is not only influenced by itself but also by environmental and mechanical factors.

Methods

Culture and maintenance of hESCs

H1 (WA-01) and H7 (WA-07) hESCs from WiCell (https://www.wicell.org/) were routinely cultured on Matrigel-coated plates in hESC culture medium MEF-CM supplemented with 10 ng/ml of bFGF (PeproTech) - with daily medium refreshment. MEF-CM was produced by incubating knockout serum replacement (KSR) medium (Knockout DMEM containing 20% KSR, 1 mM L-glutamine, 1% non-essential amino acid, 0.1 M β-mercaptoethanol, 1% Penicillin-Streptomycin, 4 ng/ml bFGF) with MEF for 24 hours as previously described[20]. hESCs were routinely propagated at ~90% confluence by collagenase-assisted mechanical splitting in which hESCs were treated with collagenase IV (200 U/ml) for 5-7 min, then removing the collagenase and washing the cells with PBS before dissecting and scraping the hESC colonies into small clumps in MEF-CM and finally seeding them onto new Matrigel-coated plates in 1:3 ratio. When required, hESCs were also dissociated into single cells by Accutase (Merck). All reagents were from Thermo Fisher Scientific unless stated. All hESC lines have been regularly tested negative for mycoplasma contamination.

Generation of RICTOR-knockout and RICTOR-knockdown hESCs

RICTOR-knockout (RIC-KO) hESCs were generated using CRISPR/Cas9 and sgRNA targeting technology. The targeting vector, eSpCas9(1.1)-2A-Puro, was constructed by replacing the Cas9 in pSpCas9(BB)-2A-Puro (PX459) with Cas9(1.1) from eSpCas9(1.1) to increase targeting specificity and both the plasmids were gifts to Addgene from Feng Zhang[53,54]. The sgRNAs were designed to target exon 4 or 5 of the RICTOR gene using two online tools, "CRISPR DESIGN" (http://crispr.mit.edu/) and "DESKGEN" (https://www.deskgen.com/landing/) and cloned into the targeting vector. The targeting efficiency of these sgRNAs were validated in HEK293T cells and two sgRNAs, one targeting exon 4 and the other targeting exon 5, were selected for co-transfection into H1 hESCs using the NeonTM Transfection system (Thermo Fisher Scientific) following the manufacturer's instruction (Supplementary Fig. 1a,b). Briefly, 1 x 10^5 Accutase-dissociated single cells of hESCs were mixed with 0.5 µg plasmids in the recommended buffer and electroporated at 1050V, 30 ms pulse width for 2 pulses. H1 hESCs transfected with empty targeting vector without any sgRNA were used as controls. 48 hours after transfection, the cells were selected by puromycin (0.5 µg/ml) treatment for 2 days and expanded until formation of colonies. Individual colonies were picked and screened for the RICTOR expression by immunoblot. The colonies with no detectable RICTOR were dissociated with Accutase and seeded in low density for second round of clonal isolation and screening. The RICTOR-negative clones were then expanded as RIC-KO hESC lines. The two sgRNA sequences are GGCCACAGTGAAGAAAAACTGGG and AGACTCCAGTATTCTCCAGA-AGG with PAM region underlined.

RICTOR-knockdown hESCs were established by transducing H7 hESCs with Rictor_2 shRNA (Addegene) lentivirus produced in HEK293T cells as previously described[51,55]. Briefly, lentiviruses were produced by transient transfection of HEK293T cells with 45 µg the above lentivector as well as 30 µg pCMVΔ8.91 helper and 15 µg pVSV-G envelope plasmids. hESCs were dissociated with Accutase into single cells and 2.5 x 10^5 hESCs were re-suspended in hESC culture medium supplemented with 10 µM ROCKi (Y-27632, Cell Guidance Systems) and infected overnight with 1.5-2 x 10^6 viral particles at the same time as when they were plated down. 48 hours post-infection, cells were selected with puromycin (5 µg/ml) for a week.

Differentiation via Embryoid body (EB) formation

EB formation was performed using AggreWell™ 400 plate (StemCell Technologies). The plate was prepared by adding anti-adherent rinsing solution and centrifuged the plate at 13,00 g for 5 minutes and meanwhile hESCs were dissociated by Accutase into single cells. After removal of the anti-adherent rinsing solution, 7-8 x 10^5 hESCs in EB medium

(DMEM/F12 containing 20% fetal bovine serum or KSR, 1 mM Glutamine,1% Penicillin-Streptomycin, 1:100 N2 and 1:200 B27) were seeded into one well of the AggreWell™400 plate in the presence of 10 µM ROCKi. The plate was carefully centrifugated for 3 minutes at 100 g to allow the formation of cell aggregates and then incubated at 37°C with 5% CO2 overnight. ROCKi was removed from the medium and the cell aggregates were gently transferred to a low attachment plate the following day and cultured for another 5 days in suspension culture with medium change every 2-3 days. The resulting embryoid bodies were then transferred to Matrigel-coated culture dish for further differentiation of 7 days (Supplementary Fig. 2e).

BMP4-induced mesendoderm differentiation

In colony forms: this differentiation method was modified from previous published ones[56,57]. Briefly, WT and RIC-KO hESCs were dissociated with the collagenase-assisted mechanical method as described above and the resulting small clusters of cells were seeded at 1:5 splitting ratio in hESC culture medium and 10 µM ROCKi was added into the medium to aid the attachment, then was withdrawn the next day. On the following day, the cells were refreshed with hESC culture medium supplemented with 50 ng/ml BMP4 alone or combined with 50 ng/ml AA, or/and 6 µM CHIR and continuously cultured for 48 hours before collection for analysis (Fig. 4e).

In spheroids: hESCs were dissociated into single cells by Accutase and 5 x105 cell^{s} per well were seeded into AggreWell™400 plate in hESC culture medium containing 10 µM ROCKi and centrifuged for 3 minutes at 100 g. The cell aggregates were refreshed with hESC culture medium supplemented with 1 ng/ml BMP4 and 10 µM ROCKi and cultured for 48 hours (Fig. 4c).

In single cells: Accutase-dissociated hESC single cells were seeded into Matrigel-coated plates at 1 x 10^5/cm^2 in hESC culture medium containing 10 µM ROCKi. The medium was replaced by fresh hESC culture medium containing 50 ng/ml BMP4 and the cells were differentiated for 48 hours.

Cell Adhesion assay

Both WT and RIC-KO hESCs were dissociated into single cells with Accutase and seeded at 2.5 x 10^4 cells/well into Matrigel-coated 96-well plate in hESC culture medium containing 2.5-10 µM ROCKi. The hESCs were then incubated at 37°C, 5% CO2 for 10 min. After removing the medium and washing with PBS, the hESCs were stained with 200 µl 0.2% crystal violet solution (Merck) for 10 minutes at room temperature. The plates were carefully washed twice with tap water and drained on paper towel before adding 100 µl of 1% SDS

into each well and incubating for 15 minutes on a shaker. Finally, the absorbance was recorded at a wavelength of 570 nm on an Optimax Tuneable microplate reader (Bio-Rad).

Alkaline phosphatase colony formation assay and CCK8 assay

hESCs were dissociated with Accutase into single cells. 6 x 10^3 hESCs were seeded on mitotically inactivated MEF feeder in a well of 12-well plates and cultured in hESC culture medium for five days before subjected to alkaline phosphatase staining using Leukocyte Alkaline Phosphatase Kit (Merck) following manufacturer's instruction. The number of positive colonies were counted from images captured under a microscope. Cell proliferation was measured using Cell Counting Kit-8 (CCK-8) from APExBIO following the manufacturer's instructions and using Sunrise absorbance microplate reader.

Reverse-Transcription-qPCR (RT-qPCR)

Total RNAs were isolated from cells with TRI-Reagent® (Merck) and cDNAs were synthesized from 2 µg total RNA with Superscript II reverse transcriptase (New England Biolabs). RT-qPCR was performed in a StepOnePlus™ Real-Time PCR System (Applied BioSystems) using SYBR® Green JumpstartTM Taq Ready Mix (Merck). A list of primer sequences is provided in the Supplementary Table 4.

RNA-sequencing (RNA-seq) analysis

Total RNA was extracted from cells by TRIzolTM Plus RNA Purification Kit (Thermo Fisher Scientific) according to the manufacturer's instruction. Library preparation, sequencing, and initial quality check were performed by Imperial BRC Genomics Facility (IGF). Libraries were prepared as strand-specific and sequenced on Illumina HiSeq 4000 (2 x 75 bp) to a depth of 30 million reads. Raw fastq format data were trimmed by Fastp v0.23.2[58] to remove sequencing adaptors and low-quality bases (< Q15). The human genome FASTA file (GRCh38 release 104) and gene annotation GTF file (GRCh38 release 104) were obtained from Ensembl and STAR v2.7.10a[59] was then used to create genome mapping indices. The expression of genes and transcripts was quantified by RSEM v1.3.3[60]. All downstream analyses were carried out in R v4.1.2 using Bioconductor packages. After genes with no reads across all the samples were removed, variance stabilising transformation (VST) was used to correct for variance differences and limma v3.50.3[61] was used to remove the batch effect between biological replicates. Differential expression and statistical analysis were performed by DESeq2 v1.34.0[62] with a false discovery rate (FDR) threshold of 0.05. Genes with a p-adj value < 0.05 and a log2 fold change (FC) > 1 (i.e., FC > 2) were considered to be differentially expressed.

Gene ontology (GO) and Kyoto Encyclopedia of Genes and Genomes (KEGG) pathway analyses were performed with the over-representation analysis using clusterProfiler v4.2.2 in R[63]. Differentially expressed genes were first classified into either the upregulated or downregulated group and then were individually run in the program to obtain enriched GO terms and pathways. P-values were again adjusted using the Benjamini-Hochberg method with a cut-off at 0.05.

Immunoblotting

Cell lysates were isolated by lysing cells in RIPA (Radio Immunoprecipitation Assay) buffer (50 mM Tris-HCl, pH 8.0, 150 mM NaCl, 1% Nonidet-P40, 0.5% sodium deoxycholate, 0.1% SDS) supplemented with phosphatase (Na3VO4, 1:100, NaF, 1:200 or phosphatase inhibitor cocktail 2, 10 µl/ml) and protease inhibitors (phenylmethylsulphonyl fluoride in ethanol or protease inhibitor cocktail, all from Merck) and passing through a 21-gauge syringe needle several times. Cell lysates were centrifuged at 15,000 x g at 4ºC for 20 min and protein concentration was quantified using bicinchoninic acid (BCA) assay kit (Thermo Fisher Scientific). 10-25 µg of proteins were resolved in 8% SDS-PAGE gels before being transferred onto polyvinylidene (PVDF) membranes via electroblotting. Blots were probed with primary antibodies overnight at 4ºC followed by horseradish peroxidise (HRP) conjugated secondary antibodies 1 hour at room temperature before being developed via ECL (enhanced chemi-luminescent) substrate and exposure onto CL-XPosure film (Thermo Fisher Scientific). Table S5 lists all the antibodies used in this study.

Immunostaining and image analysis

hESCs cultured on Nunc Thermanox Coverslips (Thermo Fisher Scientific) were fixed for 20 mins with 4% paraformaldehyde and blocked and permeabilized with PBS containing 10% goat serum, 2.5% BSA and 0.3% Triton X-100 (Merck) for 1 hour after washing. Cells were then incubated with primary antibodies at 4ºC overnight, followed by 1 hour incubation with fluorescent conjugated secondary antibodies. After washing, cells were counterstained with 4,6-diamidino-2-phenylindol (DAPI, Merck) and mounted onto microscope slides with Mowiol 4-88 solution. Spheroids were fixed with 4% paraformaldehyde overnight at 4°C and then incubated with blocking and permeabilization buffer (see above) overnight at 4°C after 3 x 15 min washes with PBST. The spheroids were then probed with primary antibodies (Supplementary Table 5) in PBS containing 1% BSA at 4°C overnight, followed by 1 hour incubation with secondary antibodies at room temperature after PBS washing. The nuclei were counterstained by DAPI and mounted with Mowiol 4-88 solution or 10% glycerol.

All the images, except those in Supplementary Fig. 4a, were captured with a Leica SP5 II confocal fluorescent microscope. The images in Supplementary Fig. 4a were taken with Nikon Eclipse E400 microscope. Quantification of positive signals were performed using ImageJ and CellProfiler[64] software after subtracting background signals using the Rolling Ball method with a radius of 50 pixels.

Flow cytometry

hESCs were dissociated into single cells using Accutase and were incubated in 150 µl blocking buffer (PBS containing 1% FBS, 1 mM EDTA and 40% goat serum) for 15 min on ice after washing. After centrifugation at 1300 rpm for 5 min the cells were resuspended in PBS containing 2% FBS and 2 mM EDTA and incubated with primary antibody or control isotype on ice for 30 min, followed by fluorescent dye-conjugated secondary antibody on ice for 30 min in the dark after washes between. Finally, cells were loaded on a FACSCalibur flow cytometer (BD Biosciences), and data were acquired and analysed using CellQuest software.

RhoA activation assay and Rac1-GTP assay

RhoA activation assay was performed using RhoA G-LISA Activation Assay Kit – colorimetric format (Cytoskeleton Inc) following manufacturer's instruction. The signals were recorded by measuring the absorbance at 490 nm wavelength 490 nm using microplate spectro-photometer.

Rac1-GTP assay was performed using Non-radioactive Rac1 Activation Assay Kit (Merck) following manufacturer's instruction. Briefly, PAK-1 PBD magnetic beads supplied in the kit was used to pull-down Rac-GTP and cdc42-GTP from cell lysates, which were then subjected to immunoblotting with anti-Rac1 antibody.

Statistical analysis

All data are represented as the mean with error bars indicating standard deviation (SD), unless indicated otherwise, for at least three biological replicates; p-values were obtained by unpaired two-tail t test, one-way or two-way ANOVA using GraphPad Prism 9 except RNA-seq analysis.

Data availability

The RNA-sequencing datasets of wildtype and RIC-KO hESCs are available in the GEO database with accession ID GSE243723.

References

1. Aylett, C.H. *et al.* Architecture of human mTOR complex 1. *Science* **351**, 48-52 (2016).
2. Chen, X. *et al.* Cryo-EM structure of human mTOR complex 2. *Cell Res* **28**, 518-528 (2018).
3. Scaiola, A. *et al.* The 3.2-A resolution structure of human mTORC2. *Sci Adv* **6** (2020).
4. Battaglioni, S., Benjamin, D., Walchli, M., Maier, T. & Hall, M.N. mTOR substrate phosphorylation in growth control. *Cell* **185**, 1814-1836 (2022).
5. Liu, G.Y. & Sabatini, D.M. mTOR at the nexus of nutrition, growth, ageing and disease. *Nat Rev Mol Cell Biol* **21**, 183-203 (2020).
6. Kim, J. & Guan, K.L. mTOR as a central hub of nutrient signalling and cell growth. *Nat Cell Biol* **21**, 63-71 (2019).
7. Guertin, D.A. *et al.* Ablation in mice of the mTORC components raptor, rictor, or mLST8 reveals that mTORC2 is required for signaling to Akt-FOXO and PKCalpha, but not S6K1. *Developmental cell* **11**, 859-871 (2006).
8. Shiota, C., Woo, J.T., Lindner, J., Shelton, K.D. & Magnuson, M.A. Multiallelic disruption of the rictor gene in mice reveals that mTOR complex 2 is essential for fetal growth and viability. *Developmental cell* **11**, 583-589 (2006).
9. Bentzinger, C.F. *et al.* Skeletal muscle-specific ablation of raptor, but not of rictor, causes metabolic changes and results in muscle dystrophy. *Cell Metab* **8**, 411-424 (2008).
10. Cybulski, N., Polak, P., Auwerx, J., Ruegg, M.A. & Hall, M.N. mTOR complex 2 in adipose tissue negatively controls whole-body growth. *Proc Natl Acad Sci U S A* **106**, 9902-9907 (2009).
11. Godel, M. *et al.* Role of mTOR in podocyte function and diabetic nephropathy in humans and mice. *J Clin Invest* **121**, 2197-2209 (2011).
12. Hagiwara, A. *et al.* Hepatic mTORC2 activates glycolysis and lipogenesis through Akt, glucokinase, and SREBP1c. *Cell Metab* **15**, 725-738 (2012).
13. Lamming, D.W. *et al.* Rapamycin-induced insulin resistance is mediated by mTORC2 loss and uncoupled from longevity. *Science* **335**, 1638-1643 (2012).
14. Zhao, X. *et al.* Phosphoinositide-dependent kinase 1 and mTORC2 synergistically maintain postnatal heart growth and heart function in mice. *Mol Cell Biol* **34**, 1966-1975 (2014).
15. Aimi, F. *et al.* Endothelial Rictor is crucial for midgestational development and sustained and extensive FGF2-induced neovascularization in the adult. *Sci Rep* **5**, 17705 (2015).
16. Dragert, K. *et al.* Deletion of Rictor in brain and fat alters peripheral clock gene expression and increases blood pressure. *Hypertension* **66**, 332-339 (2015).
17. Zhou, J. *et al.* mTOR supports long-term self-renewal and suppresses mesoderm and endoderm activities of human embryonic stem cells. *Proc Natl Acad Sci U S A* **106**, 7840-7845 (2009).
18. Bulut-Karslioglu, A. *et al.* Inhibition of mTOR induces a paused pluripotent state. *Nature* **540**, 119-123 (2016).

19. Yang, Q., Inoki, K., Ikenoue, T. & Guan, K.L. Identification of Sin1 as an essential TORC2 component required for complex formation and kinase activity. *Genes & development* **20**, 2820-2832 (2006).

20. Noisa, P., Urrutikoetxea-Uriguen, A. & Cui, W. Generation of human embryonic stem cells carrying lineage specific reporters. *Methods Mol Biol* **690**, 95-106 (2011).

21. Burridge, K. & Wennerberg, K. Rho and Rac take center stage. *Cell* **116**, 167-179 (2004).

22. Martin, E., Ouellette, M.H. & Jenna, S. Rac1/RhoA antagonism defines cell-to-cell heterogeneity during epidermal morphogenesis in nematodes. *J Cell Biol* **215**, 483-498 (2016).

23. Rojas, A. *et al.* Gata4 expression in lateral mesoderm is downstream of BMP4 and is activated directly by Forkhead and GATA transcription factors through a distal enhancer element. *Development* **132**, 3405-3417 (2005).

24. Mukherjee, S. *et al.* Sox17 and beta-catenin co-occupy Wnt-responsive enhancers to govern the endoderm gene regulatory network. *Elife* **9** (2020).

25. Weidinger, G., Thorpe, C.J., Wuennenberg-Stapleton, K., Ngai, J. & Moon, R.T. The Sp1-related transcription factors sp5 and sp5-like act downstream of Wnt/beta-catenin signaling in mesoderm and neuroectoderm patterning. *Curr Biol* **15**, 489-500 (2005).

26. Rodaway, A. & Patient, R. Mesendoderm. an ancient germ layer? *Cell* **105**, 169-172 (2001).

27. Tyser, R.C.V. *et al.* Single-cell transcriptomic characterization of a gastrulating human embryo. *Nature* **600**, 285-289 (2021).

28. Simunovic, M. *et al.* A 3D model of a human epiblast reveals BMP4-driven symmetry breaking. *Nat Cell Biol* **21**, 900-910 (2019).

29. Nowotschin, S. & Hadjantonakis, A.K. Guts and gastrulation: Emergence and convergence of endoderm in the mouse embryo. *Curr Top Dev Biol* **136**, 429-454 (2020).

30. Cui, G. *et al.* Spatial molecular anatomy of germ layers in the gastrulating cynomolgus monkey embryo. *Cell Rep* **40**, 111285 (2022).

31. Yoney, A., Bai, L., Brivanlou, A.H. & Siggia, E.D. Mechanisms underlying WNT-mediated priming of human embryonic stem cells. *Development* **149** (2022).

32. Richardson, L., Wilcockson, S.G., Guglielmi, L. & Hill, C.S. Context-dependent TGFbeta family signalling in cell fate regulation. *Nat Rev Mol Cell Biol* **24**, 876-894 (2023).

33. Nusse, R. & Clevers, H. Wnt/beta-Catenin Signaling, Disease, and Emerging Therapeutic Modalities. *Cell* **169**, 985-999 (2017).

34. Etoc, F. *et al.* A Balance between Secreted Inhibitors and Edge Sensing Controls Gastruloid Self-Organization. *Developmental cell* **39**, 302-315 (2016).

35. Zhang, Z., Zwick, S., Loew, E., Grimley, J.S. & Ramanathan, S. Mouse embryo geometry drives formation of robust signaling gradients through receptor localization. *Nat Commun* **10**, 4516 (2019).

36. Martyn, I., Brivanlou, A.H. & Siggia, E.D. A wave of WNT signaling balanced by secreted inhibitors controls primitive streak formation in micropattern colonies of human embryonic stem cells. *Development* **146** (2019).

37. Sapkota, G., Alarcon, C., Spagnoli, F.M., Brivanlou, A.H. & Massague, J. Balancing BMP signaling through integrated inputs into the Smad1 linker. *Mol Cell* **25**, 441-454 (2007).

38. Chu, Q. *et al.* mTORC2/RICTOR exerts differential levels of metabolic control in human embryonic, mesenchymal and neural stem cells. *Protein Cell* **13**, 676-682 (2022).

39. Ahmed, M. & Ffrench-Constant, C. Extracellular Matrix Regulation of Stem Cell Behavior. *Curr Stem Cell Rep* **2**, 197-206 (2016).

40. Kalluri, R. & McAndrews, K.M. The role of extracellular vesicles in cancer. *Cell* **186**, 1610-1626 (2023).

41. Jaffe, A.B. & Hall, A. Rho GTPases: biochemistry and biology. *Annu Rev Cell Dev Biol* **21**, 247-269 (2005).

42. Heasman, S.J. & Ridley, A.J. Mammalian Rho GTPases: new insights into their functions from in vivo studies. *Nat Rev Mol Cell Biol* **9**, 690-701 (2008).

43. Levay, M., Settleman, J. & Ligeti, E. Regulation of the substrate preference of p190RhoGAP by protein kinase C-mediated phosphorylation of a phospholipid binding site. *Biochemistry* **48**, 8615-8623 (2009).

44. Griner, E.M., Churchill, M.E., Brautigan, D.L. & Theodorescu, D. PKCalpha phosphorylation of RhoGDI2 at Ser31 disrupts interactions with Rac1 and decreases GDI activity. *Oncogene* **32**, 1010-1017 (2013).

45. Morrison, M.M. *et al.* mTOR Directs Breast Morphogenesis through the PKC-alpha-Rac1 Signaling Axis. *PLoS Genet* **11**, e1005291 (2015).

46. Ikenoue, T., Inoki, K., Yang, Q., Zhou, X. & Guan, K.L. Essential function of TORC2 in PKC and Akt turn motif phosphorylation, maturation and signalling. *EMBO J* **27**, 1919-1931 (2008).

47. Agarwal, N.K. *et al.* Rictor regulates cell migration by suppressing RhoGDI2. *Oncogene* **32**, 2521-2526 (2013).

48. Steinhart, Z. & Angers, S. Wnt signaling in development and tissue homeostasis. *Development* **145** (2018).

49. Wang, Q. *et al.* The p53 Family Coordinates Wnt and Nodal Inputs in Mesendodermal Differentiation of Embryonic Stem Cells. *Cell Stem Cell* **20**, 70-86 (2017).

50. Estaras, C., Hsu, H.T., Huang, L. & Jones, K.A. YAP repression of the WNT3 gene controls hESC differentiation along the cardiac mesoderm lineage. *Genes & development* **31**, 2250-2263 (2017).

51. Yu, J.S. *et al.* PI3K/mTORC2 regulates TGF-beta/Activin signalling by modulating Smad2/3 activity via linker phosphorylation. *Nat Commun* **6**, 7212 (2015).

52. David, C.J. & Massague, J. Contextual determinants of TGFbeta action in development, immunity and cancer. *Nat Rev Mol Cell Biol* **19**, 419-435 (2018).

53. Ran, F.A. *et al.* Genome engineering using the CRISPR-Cas9 system. *Nat Protoc* **8**, 2281-2308 (2013).

54. Slaymaker, I.M. *et al.* Rationally engineered Cas9 nucleases with improved specificity. *Science* **351**, 84-88 (2016).

55. Sarbassov, D.D., Guertin, D.A., Ali, S.M. & Sabatini, D.M. Phosphorylation and regulation of Akt/PKB by the rictor-mTOR complex. *Science* **307**, 1098-1101 (2005).

56. Bernardo, A.S. *et al.* BRACHYURY and CDX2 mediate BMP-induced differentiation of human and mouse pluripotent stem cells into embryonic and extraembryonic lineages. *Cell Stem Cell* **9**, 144-155 (2011).

57. Warmflash, A., Sorre, B., Etoc, F., Siggia, E.D. & Brivanlou, A.H. A method to recapitulate early embryonic spatial patterning in human embryonic stem cells. *Nat Methods* **11**, 847-854 (2014).

58. Chen, S., Zhou, Y., Chen, Y. & Gu, J. fastp: an ultra-fast all-in-one FASTQ preprocessor. *Bioinformatics* **34**, i884-i890 (2018).

59. Dobin, A. *et al.* STAR: ultrafast universal RNA-seq aligner. *Bioinformatics* **29**, 15-21 (2013).

60. Li, B. & Dewey, C.N. RSEM: accurate transcript quantification from RNA-Seq data with or without a reference genome. *BMC Bioinformatics* **12**, 323 (2011).

61. Ritchie, M.E. *et al.* limma powers differential expression analyses for RNA-sequencing and microarray studies. *Nucleic Acids Res* **43**, e47 (2015).

62. Love, M.I., Huber, W. & Anders, S. Moderated estimation of fold change and dispersion for RNA-seq data with DESeq2. *Genome Biol* **15**, 550 (2014).

63. Yu, G., Wang, L.G., Han, Y. & He, Q.Y. clusterProfiler: an R package for comparing biological themes among gene clusters. *OMICS* **16**, 284-287 (2012).

64. McQuin, C. *et al.* CellProfiler 3.0: Next-generation image processing for biology. *PLoS Biol* **16**, e2005970 (2018).

Acknowledgements

This research is supported by Genesis Research Trust (grant no. P64247). FB is supported by PhD scholarship from the Punjab Educational Endowment Fund and YHC is partially sponsored by GSSA scholarship. We thank the Imperial BRC Genomics Facility (IGF) for providing the RNA-sequencing service and all the members in Stem Cell Differentiation group for their helpful discussion.

Author contributions

W.C. conceived project and designed research strategy and experiments. Y.-H.C. and F.B designed gene targeting strategies and generated RIC-KO and -KD hESC lines, respectively and carried out initial characterization on them. L.T and F.B designed and performed differentiation experiments and data analysis. L.T., F.B., and X.M. performed cell culture, molecular experiments and data analysis. L.T performed RNA-seq experiments and analysis supervised by S.A. Y.Z. provided technical support for cell culture and molecular experiments. W.C. and L.T. wrote the manuscript with inputs from all authors.

Declaration of interests

The authors declare no competing interests.

Figure Legends

Fig. 1 | RICTOR-knockout hESCs retain the self-renewal and pluripotent marker expression. a-b, Representative immunoblots show the expression of mTORC1 and mTORC2 key subunits (**a**) as well as their substrates (**b**) (n > 2). Prt, H1 parental hESCs; C1 & C3, two wildtype (WT) controls; K1 & K5, two RICTOR-knockout (RIC-KO) clones. **c,** Growth and proliferation of undifferentiated hESC lines as well as their differentiated fibroblasts by CCK8 assay. Data are presented as mean ± SEM of 3 independent cultures for each line relative to 6-hour. ** & *** represent p <0.005 & 0.0005, respectively by two-way ANOVA. **d,** Representative phase-contrast images of WT and RIC-KO hESCs. Scale bar = 50 µm. **e,** mRNA expression of key pluripotent transcription factors in WT and RIC-KO hESCs by RT-qPCR. Data are presented as mean ± SD from 3 independent biological samples. **f-g,** Protein expression of key pluripotent transcription factors in WT and RIC-KO hESCs by immunoblotting (**f**) and immunostaining (**g**) (n > 2). Scale bar = 25 µm. **h,** Expression of hESC-associated cell surface antigens in WT and RIC-KO hESCs by flow cytometry (n = 2).

Fig. 2 | RIC-KO hESCs exhibit reduced cell adhesion. a, Representative images of violet staining of hESC colonies 24 hours after plating in the presence or absence of the ROCK inhibitor (ROCKi) (n = 3). **b,** Cell attachment assay with indicated concentration of ROCKi. Data are presented as mean ± SD of 4 independent biological samples for each line. *, ** & *** represent $p < 0.05$, 0.01 and 0.0005 by two-way ANOVA test. **c,** Expression of proteins associated with cell adhesion by immunoblotting (n ≥ 2). **d,** Immunostaining of WT and RIC-KO hESCs with E-CADHERIN (E-CAD) and β-CATENIN (β-CAT) antibodies. Scale bar = 30 µm. **e,** Representative phase-contrast images of two independent embryoid body (EB) formation experiments in WT and RIC-KO hESCs in the absence or presence of ROCKi (n = 2 independent EB formation). Zoomed inserts on day 3 showing blebs in RIC-KO EBs. Scale bar = 100 µm. **f,** RhoA activity in WT and RIC-KO hESCs. Data are presented as mean ± SD of 4 independent experiments. * & ** represent $p < 0.05$ and 0.005, respectively, by one-way ANOVA. **g,** Rac1-GTP in WT and RIC-KO hESCs by Rac1-GTP pull down assay (n = 2).

Fig. 3 | Alteration of developmental-associated gene expression in RIC-KO hESCs by RNA-seq analysis. a, Heatmap and hierarchical clustering showing differential expressed genes in WT and RIC-KO hESCs from two biological replicates for each line. **b,** Volcano plots showing differentially expressed genes (adjusted P value (Padj) < 0.05; log2 (fold

change) >1) in RIC-KO hESCs compared to WT controls. Blue and red dots represent downregulated and upregulated genes, respectively. **c,** Gene ontology enrichment of biological process (Padj < 0.05) showing downregulated genes in RIC-KO hESCs predominantly involved in embryonic development. **d,** Gene ontology enrichment of molecular function (Padj < 0.05) for the downregulated genes in RIC-KO hESCs. **e,** KEGG pathway enrichment (Padj < 0.05) of downregulated genes in RIC-KO hESCs.

Fig. 4 | mTORC2-deficiency impedes mesendoderm differentiation. a, Expression of the three germ layer markers 14 days after differentiation via EB formation (n = 2 independent differentiation experiments). Scale bar = 50 µm. **b,** Dynamic mRNA expression during EB differentiation by RT-qPCR. Data are presented as mean ± SD of 6 measurements of 2 independent differentiation experiments. **c,** Schematic of BMP4-induced differentiation in spheroids. **d,** Representative images of immunostaining in max intensive projection with Brachyury (BRA) and SOX2 antibodies in (left, scale bar = 75 µm) and quantitative analysis of % BRA+ cells per colony (right). **e,** Schematic of BMP4-induced differentiation in hESC colonies. **f,** Representative images of immunostaining with Brachyury (BRA) and SOX2 antibodies (left, scale bar = 250 µm) and quantitative analysis (right). The quantification in c & d is presented as mean ± SD with each symbol representing a colony and the total number of colonies analyzed for each line is indicated in the bracket from 3 independent differentiation experiments. *** $p < 0.0001$ by one-way ANOVA.

Fig. 5 | Activation of WNT considerably improves mesendoderm differentiation in RIC-KO hESCs. Representative immunostaining images of Brachyury (BRA) and SOX2 (left, Scale bar = 250 µm) from differentiation experiments induced by a combination of indicated growth factors/small molecule with quantitative analysis (right): **a,** BMP4 together with Activin A (AA) and CHIR99021 (CHIR); **b,** BMP4 and AA; **c,** BMP4 and CHIR; **d,** CHIR only. Quantification is presented as median with 95% confidence interval and each symbol represents a colony and the total number of colonies analyzed for each cell line is indicated in the bracket from 3 independent experiments. ** and *** $p < 0.005$ and 0.0005, respectively, by one-way ANOVA.

Fig. 6 | BMP4-induced activation of WNT is hampered in RIC-KO hESCs. a, Representative Immunoblot images showing indicated protein expression in WT and RIC-KO hESCs at indicated timepoints during BMP4-induced differentiation (n = 2 independent

differentiation). The number below the images represent ratio of the protein above to its housekeeping protein below calculated by densitometry from ImageJ. **b,** Expression of genes associated with WNT signaling during BMP4-induced mesendoderm differentiation by RT-qPCR in WT and RIC-KO hESCs. Data are presented as mean ± SD of 3 independent differentiation experiments. ** and *** $p < 0.005$ and 0.0005, respectively, by two-way ANOVA. **c,d,** Immunostaining with indicated antibodies at indicated timepoints of BMP4-induced differentiation in C1 and K1 hESCs. Scale bar = 100 µm. Dash lines indicate the boundary of intense E-CAD staining (n = 3 independent differentiation experiments).

Fig. 7 | Cell-cell interaction promotes the BMP4-induced activation of WNT in hESCs. a, Schematic of experimental procedure in colony (CL)- and single cells (SC)-plated hESCs. **b,** Immunostaining with Brachyury and SOX2 antibodies in indicated cells as shown in (a) at 48 hours of BMP4-induced differentiation. Scale bar = 100 µm. **c,** Immunostaining with pSMAD1and E-CAD antibodies in indicated cells at indicated timepoints of BMP4-induced differentiation (n = 3). **d,** Comparing the expression of genes associated with WNT signaling during BMP4-induced differentiation in CL vs SC WT hESCs by RT-qPCR. Data are presented as mean ± SD of 3 independent differentiation experiments. ** and *** $p < 0.005$ and 0.0005, respectively, by two-way ANOVA.

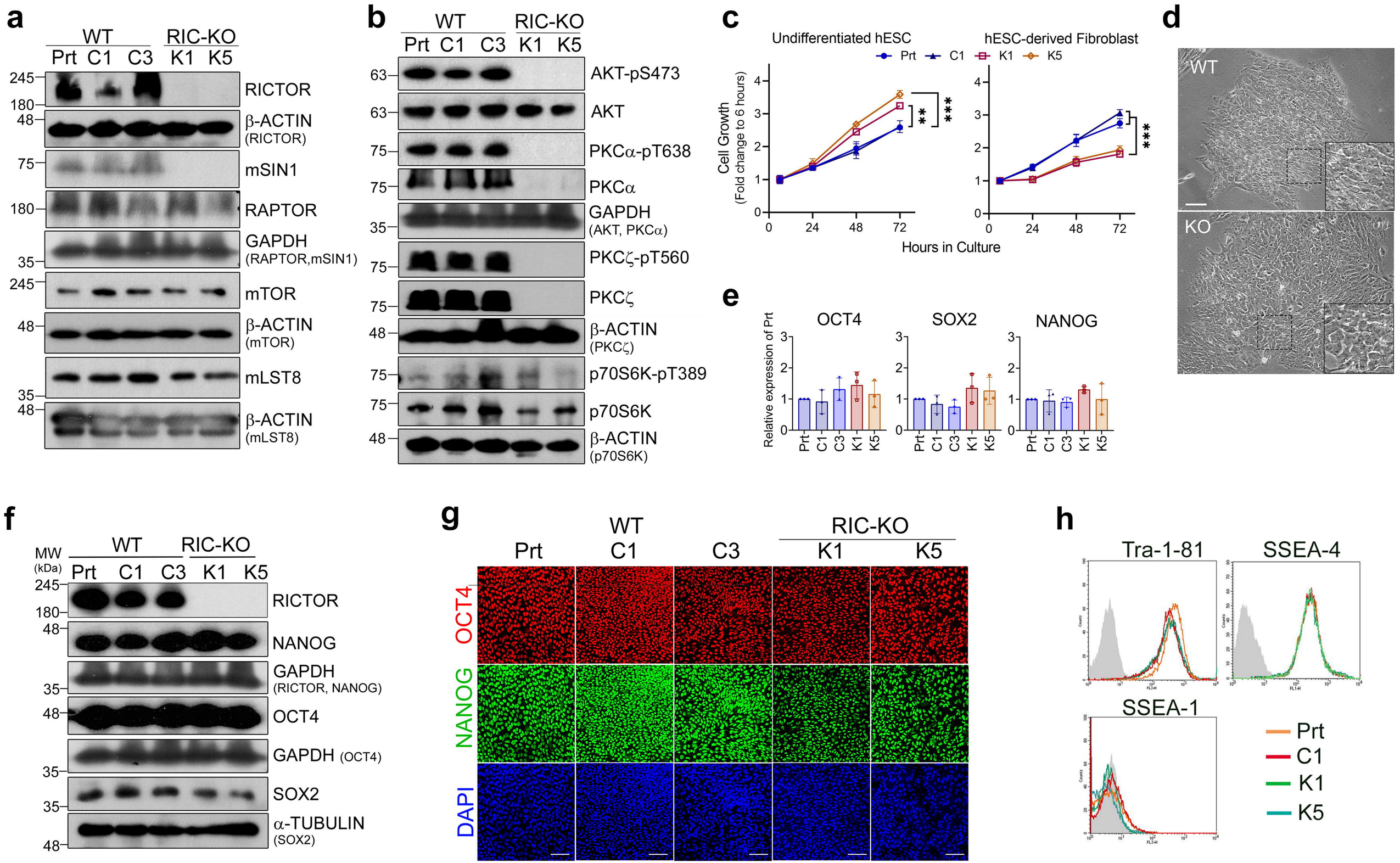
a
WT
RIC-KO
Prt C1 C3 K1 K5
245
180
48
75
180
35
245
48
35
48
RICTOR
β-ACTIN (RICTOR)
mSIN1
RAPTOR
GAPDH (RAPTOR,mSIN1)
mTOR
β-ACTIN (mTOR)
mLST8
β-ACTIN (mLST8)
b
WT
RIC-KO
Prt C1 C3 K1 K5
63
63
75
75
35
75
75
48
75
75
48
AKT-pS473
AKT
PKCα-pT638
PKCα
GAPDH (AKT, PKCα)
PKCζ-pT560
PKCζ
β-ACTIN (PKCζ)
p70S6K-pT389
p70S6K
β-ACTIN (p70S6K)
c
Undifferentiated hESC
hESC-derived Fibroblast
Prt C1 K1 K5
Cell Growth (Fold change to 6 hours)
Hours in Culture
0 24 48 72
**
***
d
WT
KO
e
OCT4
SOX2
NANOG
Relative expression of Prt
Prt C1 C3 K1 K5
f
MW (kDa)
WT
RIC-KO
Prt C1 C3 K1 K5
245
180
48
35
48
35
35
48
RICTOR
NANOG
GAPDH (RICTOR, NANOG)
OCT4
GAPDH (OCT4)
SOX2
α-TUBULIN (SOX2)
g
Prt
WT C1
C3
RIC-KO K1 K5
OCT4
NANOG
DAPI
h
Tra-1-81
SSEA-4
SSEA-1
Prt
C1
K1
K5

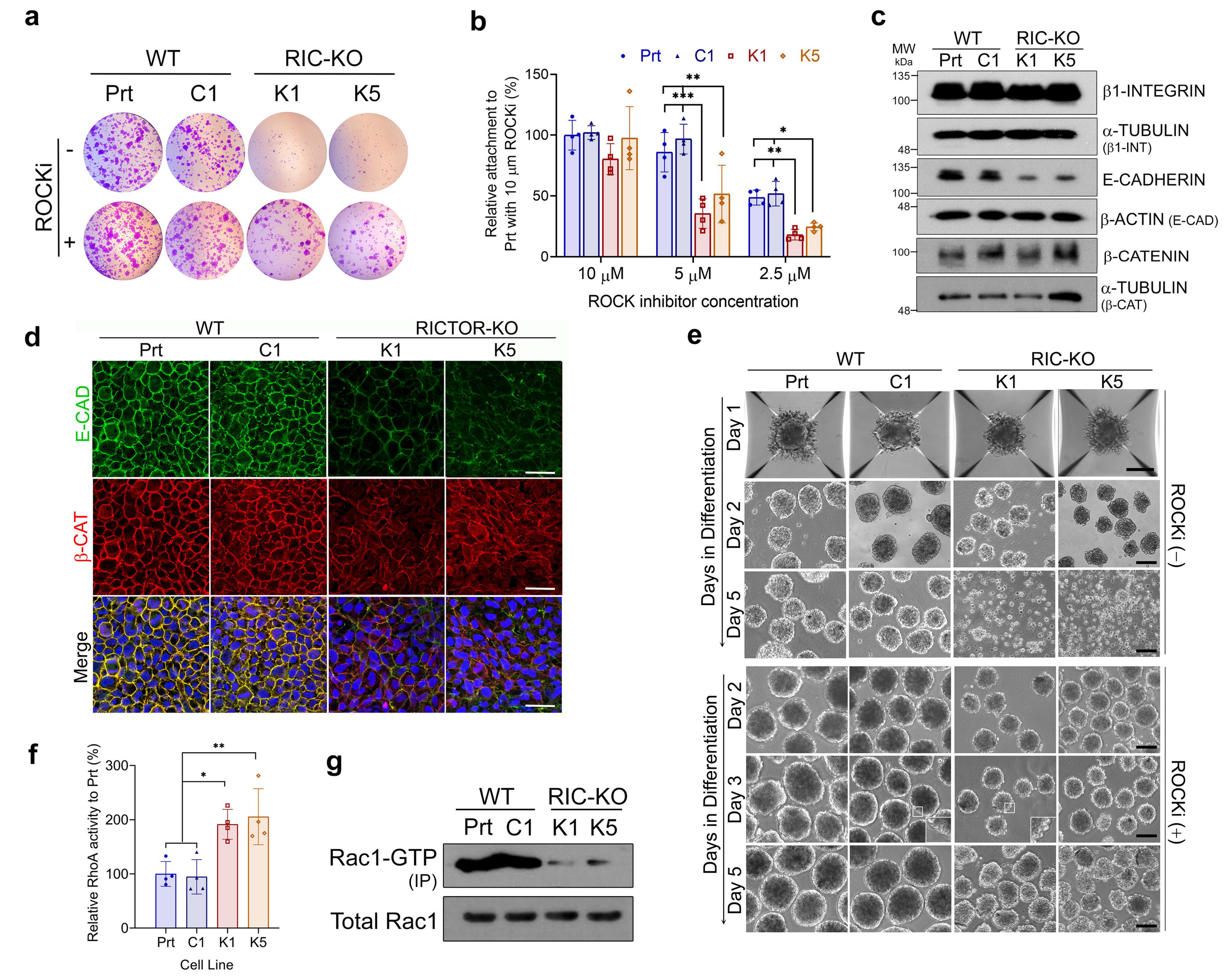
a
WT
RIC-KO
Prt
C1
K1
K5
ROCKi
-
+
b
Prt
C1
K1
K5
Relative attachment to Prt with 10 μm ROCKi (%)
150
100
50
0
**
***
*
**
10 μM
5 μM
2.5 μM
ROCK inhibitor concentration
c
MW kDa
WT
RIC-KO
Prt
C1
K1
K5
135
100
48
β1-INTEGRIN
α-TUBULIN (β1-INT)
E-CADHERIN
β-ACTIN (E-CAD)
β-CATENIN
α-TUBULIN (β-CAT)
d
WT
RICTOR-KO
Prt
C1
K1
K5
E-CAD
β-CAT
Merge
e
WT
RIC-KO
Prt
C1
K1
K5
Days in Differentiation
Day 1
Day 2
Day 5
ROCKi (−)
Day 2
Day 3
Day 5
ROCKi (+)
f
Relative RhoA activity to Prt (%)
300
200
100
0
**
*
Prt
C1
K1
K5
Cell Line
g
WT
RIC-KO
Prt
C1
K1
K5
Rac1-GTP (IP)
Total Rac1

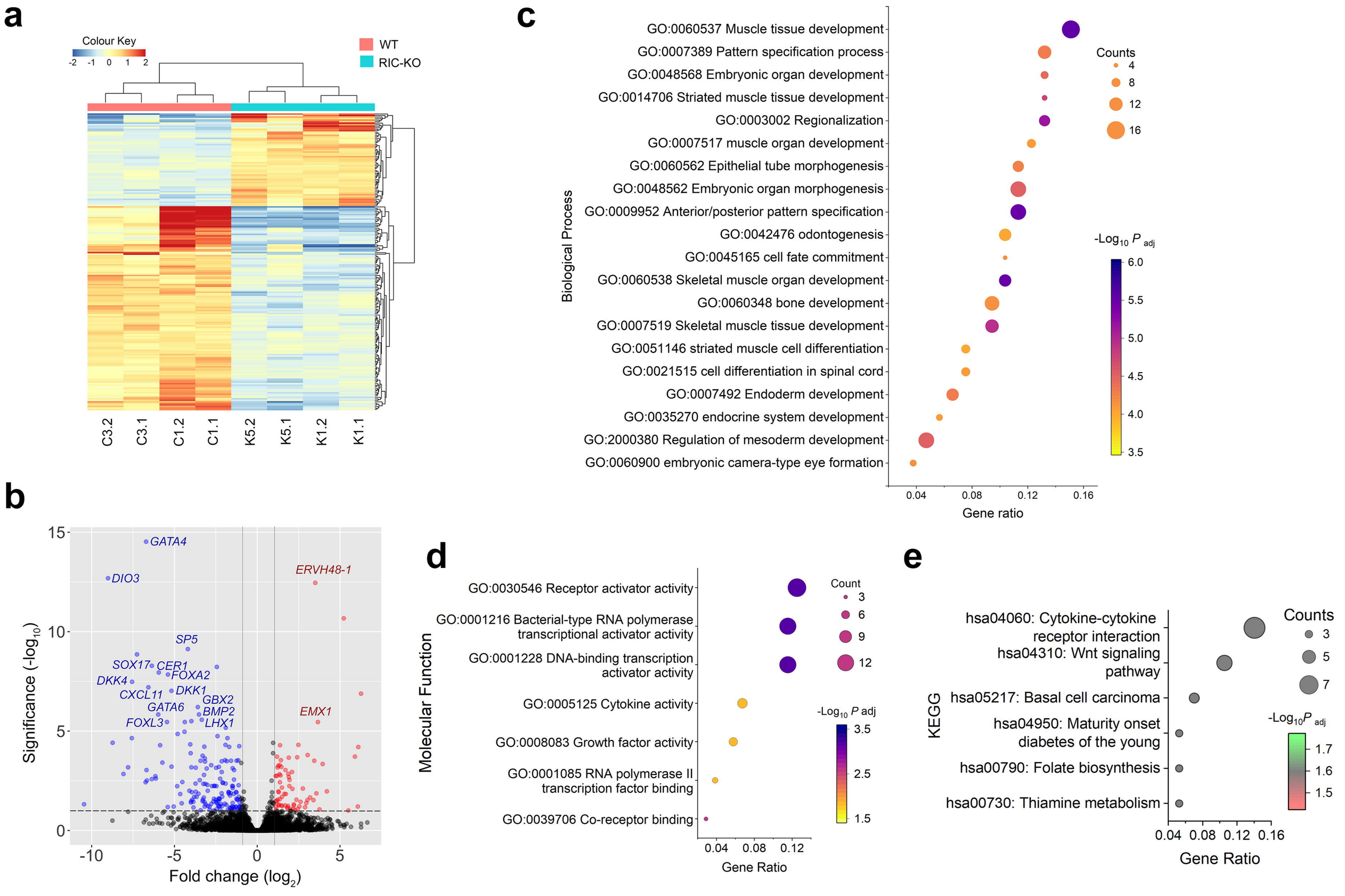
a
Colour Key
-2 -1 0 1 2
WT
RIC-KO
C3.2
C3.1
C1.2
C1.1
K5.2
K5.1
K1.2
K1.1
b
GATA4
DIO3
ERVH48-1
SP5
SOX17
CER1
FOXA2
DKK4
CXCL11
DKK1
GBX2
GATA6
BMP2
FOXL3
LHX1
EMX1
Significance (-log10)
Fold change (log2)
c
GO:0060537 Muscle tissue development
GO:0007389 Pattern specification process
GO:0048568 Embryonic organ development
GO:0014706 Striated muscle tissue development
GO:0003002 Regionalization
GO:0007517 muscle organ development
GO:0060562 Epithelial tube morphogenesis
GO:0048562 Embryonic organ morphogenesis
GO:0009952 Anterior/posterior pattern specification
GO:0042476 odontogenesis
GO:0045165 cell fate commitment
GO:0060538 Skeletal muscle organ development
GO:0060348 bone development
GO:0007519 Skeletal muscle tissue development
GO:0051146 striated muscle cell differentiation
GO:0021515 cell differentiation in spinal cord
GO:0007492 Endoderm development
GO:0035270 endocrine system development
GO:2000380 Regulation of mesoderm development
GO:0060900 embryonic camera-type eye formation
Biological Process
Gene ratio
Counts
-Log10 P adj
d
GO:0030546 Receptor activator activity
GO:0001216 Bacterial-type RNA polymerase transcriptional activator activity
GO:0001228 DNA-binding transcription activator activity
GO:0005125 Cytokine activity
GO:0008083 Growth factor activity
GO:0001085 RNA polymerase II transcription factor binding
GO:0039706 Co-receptor binding
Molecular Function
Gene Ratio
Count
-Log10 P adj
e
hsa04060: Cytokine-cytokine receptor interaction
hsa04310: Wnt signaling pathway
hsa05217: Basal cell carcinoma
hsa04950: Maturity onset diabetes of the young
hsa00790: Folate biosynthesis
hsa00730: Thiamine metabolism
KEGG
Gene Ratio
Counts
-Log10P adj

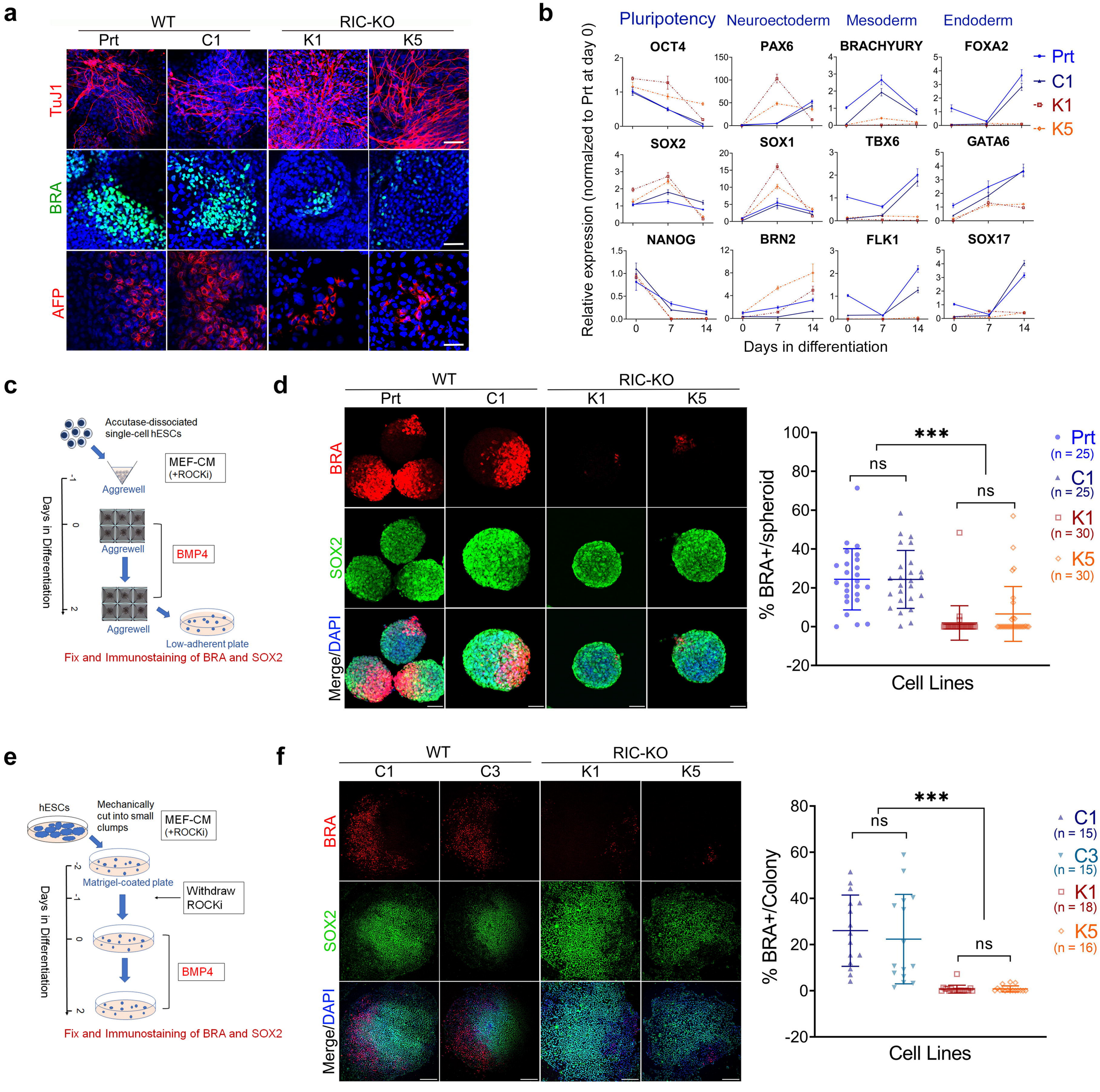
a
WT
RIC-KO
Prt
C1
K1
K5
TuJ1
BRA
AFP
b
Pluripotency
Neuroectoderm
Mesoderm
Endoderm
OCT4
PAX6
BRACHYURY
FOXA2
SOX2
SOX1
TBX6
GATA6
NANOG
BRN2
FLK1
SOX17
Prt
C1
K1
K5
Relative expression (normalzed to Prt at day 0)
Days in differentiation
c
Accutase-dissociated single-cell hESCs
MEF-CM (+ROCKi)
Aggrewell
Aggrewell
BMP4
Aggrewell
Low-adherent plate
Days in Differentiation
Fix and Immunostaining of BRA and SOX2
d
WT
RIC-KO
Prt
C1
K1
K5
BRA
SOX2
Merge/DAPI
% BRA+/spheroid
***
ns
ns
Cell Lines
Prt (n = 25)
C1 (n = 25)
K1 (n = 30)
K5 (n = 30)
e
hESCs
Mechanically cut into small clumps
MEF-CM (+ROCKi)
Matrigel-coated plate
Withdraw ROCKi
BMP4
Days in Differentiation
Fix and Immunostaining of BRA and SOX2
f
WT
RIC-KO
C1
C3
K1
K5
BRA
SOX2
Merge/DAPI
% BRA+/Colony
***
ns
ns
Cell Lines
C1 (n = 15)
C3 (n = 15)
K1 (n = 18)
K5 (n = 16)

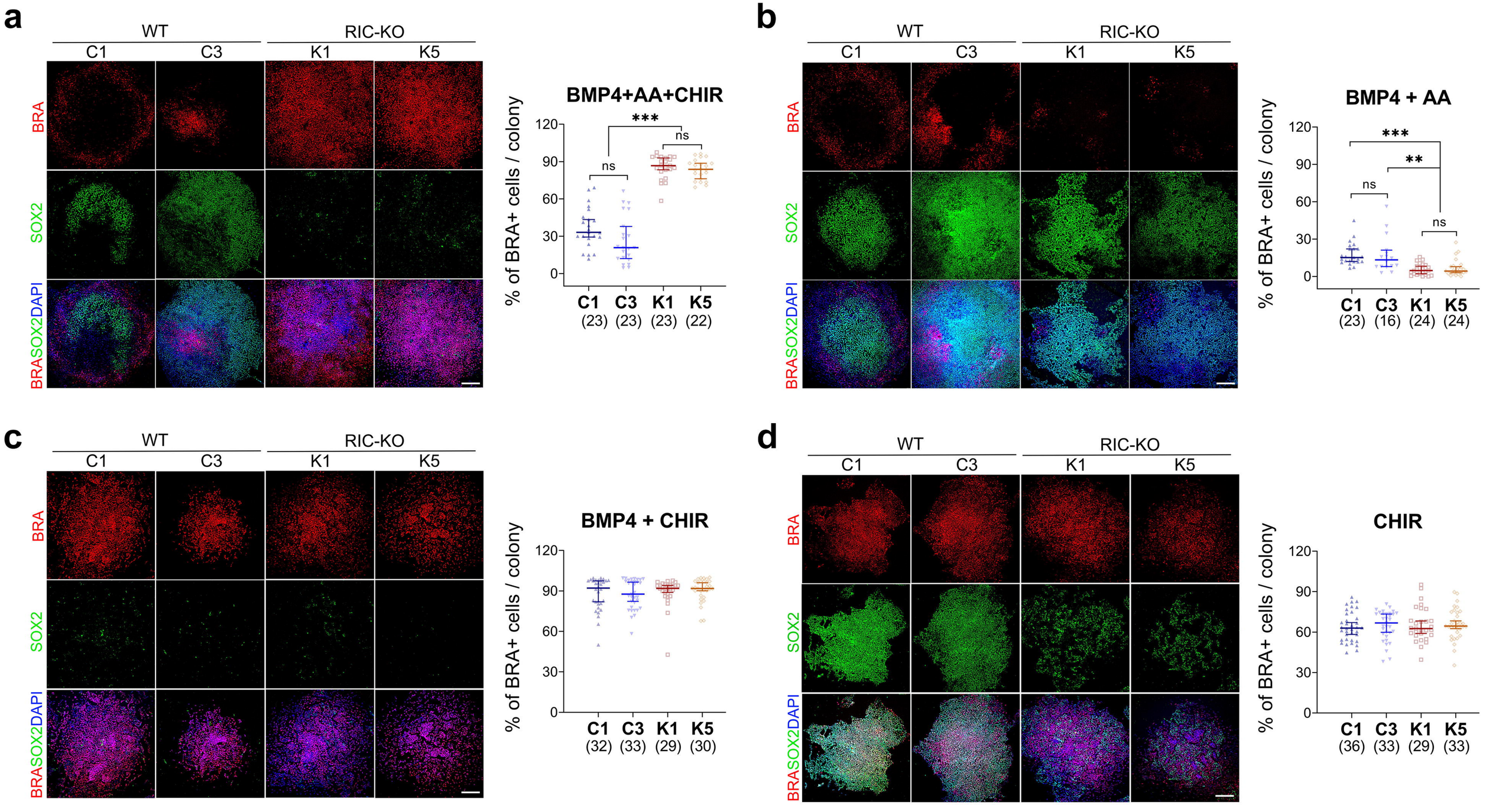
a
WT
RIC-KO
C1
C3
K1
K5
BRA
SOX2
BRASOX2DAPI
BMP4+AA+CHIR
% of BRA+ cells / colony
***
ns
ns
C1 (23)
C3 (23)
K1 (23)
K5 (22)
b
BMP4 + AA
***
**
ns
ns
C1 (23)
C3 (16)
K1 (24)
K5 (24)
c
BMP4 + CHIR
C1 (32)
C3 (33)
K1 (29)
K5 (30)
d
CHIR
C1 (36)
C3 (33)
K1 (29)
K5 (33)

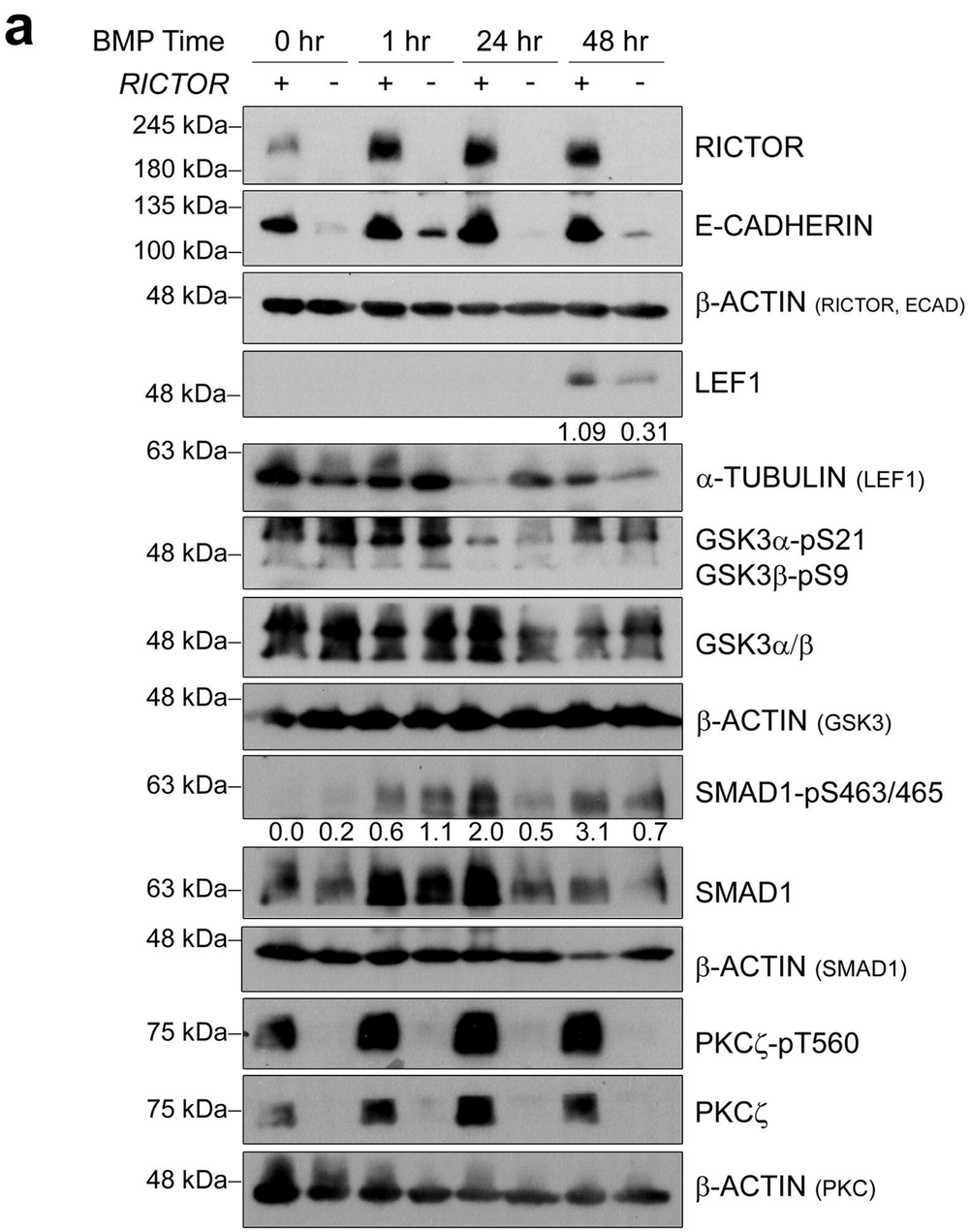
a
BMP Time
0 hr
1 hr
24 hr
48 hr
RICTOR
+ - + - + - + -
245 kDa
180 kDa
RICTOR
135 kDa
100 kDa
E-CADHERIN
48 kDa
β-ACTIN (RICTOR, ECAD)
48 kDa
LEF1
1.09 0.31
63 kDa
α-TUBULIN (LEF1)
48 kDa
GSK3α-pS21
GSK3β-pS9
48 kDa
GSK3α/β
48 kDa
β-ACTIN (GSK3)
63 kDa
SMAD1-pS463/465
0.0 0.2 0.6 1.1 2.0 0.5 3.1 0.7
63 kDa
SMAD1
48 kDa
β-ACTIN (SMAD1)
75 kDa
PKCζ-pT560
75 kDa
PKCζ
48 kDa
β-ACTIN (PKC)

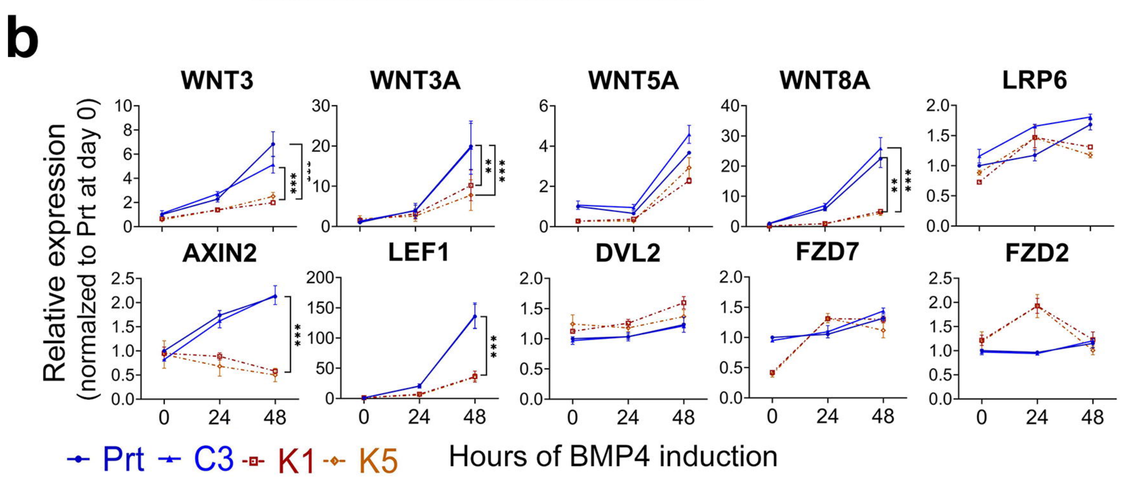
b
WNT3
WNT3A
WNT5A
WNT8A
LRP6
AXIN2
LEF1
DVL2
FZD7
FZD2
Relative expression
(normalzed to Prt at day 0)
0 24 48
Prt C3 K1 K5
Hours of BMP4 induction

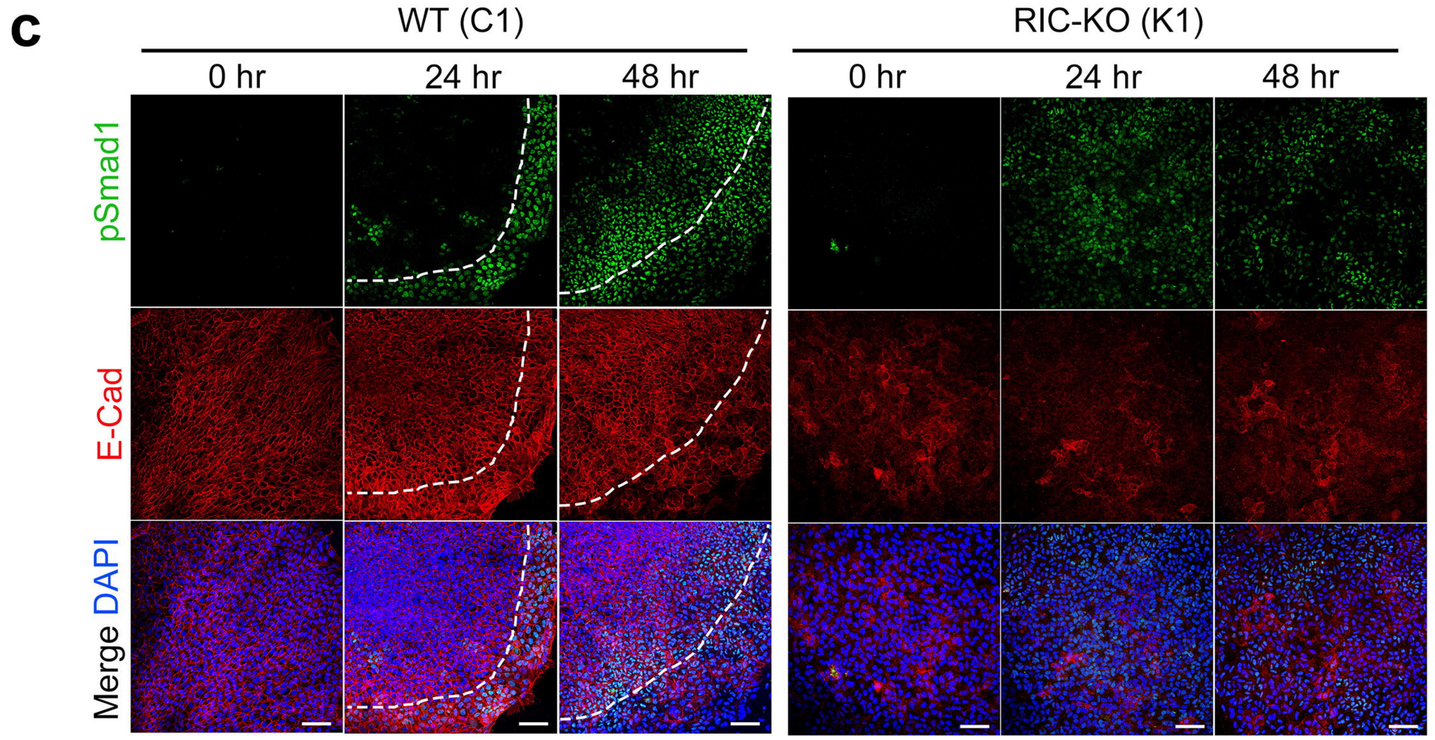
c
WT (C1)
RIC-KO (K1)
0 hr
24 hr
48 hr
pSmad1
E-Cad
Merge DAPI

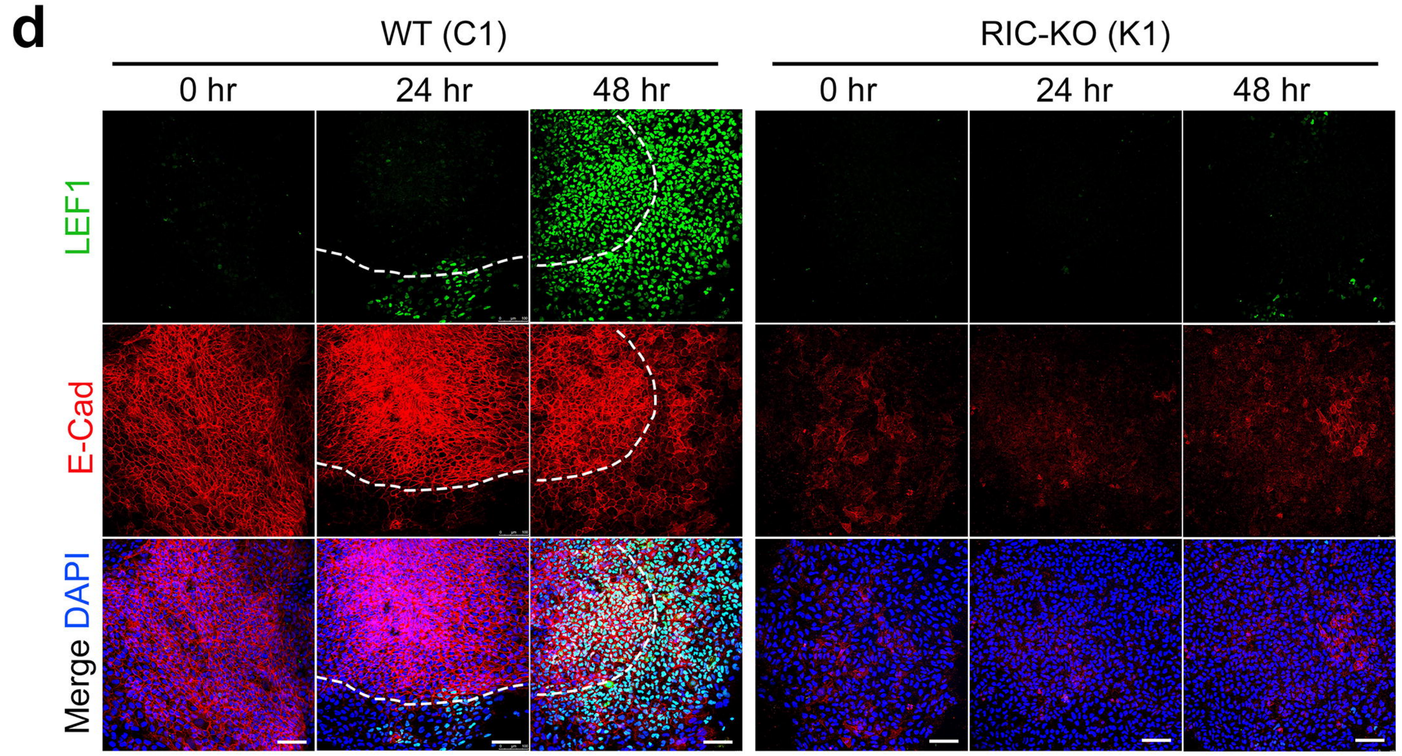
d
WT (C1)
RIC-KO (K1)
0 hr
24 hr
48 hr
LEF1
E-Cad
Merge DAPI

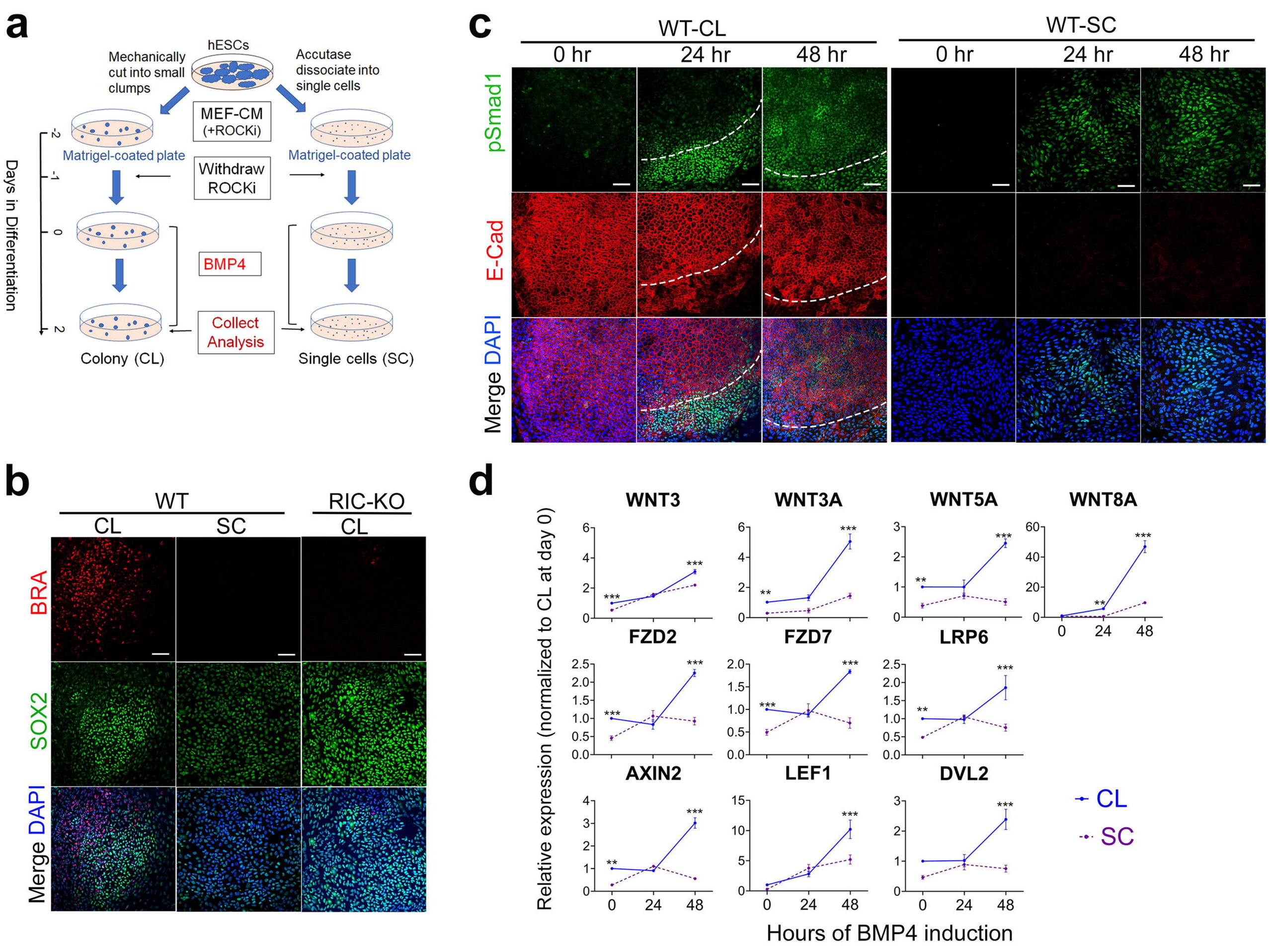
a
hESCs
Mechanically cut into small clumps
Accutase dissociate into single cells
MEF-CM (+ROCKi)
Matrigel-coated plate
Matrigel-coated plate
Withdraw ROCKi
BMP4
Collect Analysis
Days in Differentiation
-2
-1
0
2
Colony (CL)
Single cells (SC)
b
WT
RIC-KO
CL
SC
CL
BRA
SOX2
Merge DAPI
c
WT-CL
WT-SC
0 hr
24 hr
48 hr
0 hr
24 hr
48 hr
pSmad1
E-Cad
Merge DAPI
d
WNT3
WNT3A
WNT5A
WNT8A
FZD2
FZD7
LRP6
AXIN2
LEF1
DVL2
Relative expression (normalized to CL at day 0)
Hours of BMP4 induction
CL
SC